Advances in Science and Technology Research Journal

Advances in Science and Technology Research Journal, 2026, 20(3), 396–408
https://doi.org/10.12913/22998624/213435
ISSN 2299-8624, License CC-BY 4.0

Received: 2025.10.02
Accepted: 2025.12.16
Published: 2026.02.01

Evaluation of soil-tool interaction in excavation through smoothed particle hydrodynamics – based numerical modeling and laboratory validation

Hibat Rahmane Bakhouche[1*], Belkacem Meddour[2], Hamma Zedira[3], Mohammed Salah Aggoune[4]

[1] Department of Mechanical Engineering, Laboratory of Structures, Atomic Interatomic Properties and Interactions (LASPI2A), University of Abbas Laghrour, Khenchela, Algeria
[2] Department of Mechanical Engineering, Laboratory of Advanced Materials Science and Engineering (ISMA), University of Abbas Laghrour, Khenchela, Algeria
[3] Department of Civil Engineering, Laboratory of Structures, Atomic Interatomic Properties and Interactions (LASPI2A), University of Abbas Laghrour, Khenchela, Algeria
[4] Department of Mechanical Engineering, Echahid Cheikh Larbi Tebessi University, Tebessa, Algeria
* Corresponding author's e-mail: hiba.bakhouche@univ-khenchela.dz

ABSTRACT

Excavation efficiency is strongly influenced by tool geometry and operating conditions. This study applied three-dimensional modeling with the smoothed particle hydrodynamics method by implementing the Mohr-Coulomb (MC) soil model in Abaqus Explicit to analyze the effect of rake angle and excavation depth on the performance of a bucket tooth operating in clayey sand. Simulations covered rake angles between 30° and 90° and depths up to 300 mm, assessing reaction forces and displacement. Results show that reaction forces rise with increasing depth, while optimal performance occurs at rake angles between 30° and 60°. Within this range, the bucket tooth achieved efficient soil displacement and reduced cutting resistance, with the 45 degree angle and 100 mm depth configuration providing the best balance between the minimized reaction forces and effective material removal. These outcomes highlight the importance of selecting appropriate rake angles and excavation depths to achieve lower energy demands and improved operational performance in excavation systems.

Keywords: excavation tool, rake angle, soil-tool interaction, smoothed particle hydrodynamics.

INTRODUCTION

Excavation and dredging are central processes in civil and geotechnical engineering, where efficiency and reliability depend strongly on the interaction between soil and excavation tools. Whether applied to foundation construction, tunneling, or resource extraction, understanding this interaction is critical for ensuring project success and reducing operational costs [1, 2]. The process is highly complex and dynamic, shaped by soil properties, excavation speed, tool geometry, and material characteristics [3]. Accurately modeling soil-tool interaction remains a major challenge because excavation involves large soil deformations, free soil surfaces, and rapidly changing forces at the soil-tool interface [4, 5]. The problem is further complicated by the natural variability of soil, the nonlinear response of which depends on factors such as moisture content, composition, and cohesion [6–9]. For instance, unconsolidated sandy soils exhibit responses that differ significantly from cohesive clays when subjected to excavation-induced stresses [10, 11].

Historically, experimental methods such as soil bin tests have played a crucial role in studying tool performance and soil interaction, offering valuable empirical data despite their inability to fully capture the complexity of these interactions [12]. To complement experimental studies, engineers have increasingly adopted numerical techniques, such as the finite element method (FEM) to simulate the soil behavior under excavation forces, allowing detailed analysis of tool response, soil deformation, and associated stresses [13, 14]. FEM-based constitutive models provide insights into stress distribution, wear characteristics, and energy consumption during soil cutting [15], while also capturing dynamic factors, such as excavation velocity, which significantly affect cutting forces and soil deformation patterns [16].

Among constitutive models, the Mohr-Coulomb (MC) model is one of the most widely used due to its efficiency in representing soil shear strength and failure under combined normal and shear stresses [6, 17]. Extensions such as the Modified Mohr-Coulomb (MMC) model incorporate nonlinear stress-strain behavior and dilatancy effects, providing improved predictions of soil stability during excavation, including complex loading and unloading scenarios [18]. The MMC model has been especially valuable for analyzing slope stability, tunneling, and foundation excavation, as well as predicting lateral earth pressures in retaining walls under layered or heterogeneous soil conditions [19].

Despite the strengths of FEM, conventional mesh-based methods face difficulties when applied to the problems involving large soil deformations and free soil surfaces. To overcome these limitations, the smoothed particle hydrodynamics (SPH) method, a mesh-free Lagrangian technique originally developed for astrophysical simulations, has emerged as an effective alternative for simulating the soil behavior under excavation conditions [4, 20]. SPH handles discontinuities and large strains without remeshing, enabling more realistic modeling of soil-tool interactions, including cutting, displacement, and failure mechanisms [10]. Recent studies integrating SPH with MC type constitutive models have shown strong agreement with soil bin test results, confirming its reliability and applicability in geotechnical engineering contexts [21].

Both experimental and numerical studies have demonstrated the critical influence of rake angle and cutting depth, on soil reaction forces and excavation efficiency [22]. These parameters directly affect soil failure patterns and cutting resistance, with implications for tool wear and energy consumption. Numerical simulations using FEM and SPH have provided valuable insights into these relationships, supporting the optimization of excavation tool design, material selection, and operating parameters [23].

This study aimed to investigate the effect of excavation tool operating conditions on soil behavior and to evaluate their influence on soil reaction forces. A clayey sand soil was selected for this purpose, and experiments were conducted in a soil bin with dimensions of 700×400×500 mm. The experimental results were compared with the numerical simulations performed using the SPH method implemented in Abaqus/Explicit. The study focused on analyzing the influence of varying rake angle and excavation depth relative to the soil bin test, where the cutting process was modeled step by step in the simulation, allowing a detailed analysis of soil displacement and reaction forces during and after excavation. The results clearly demonstrate that both rake angle and operating depth significantly affect excavation forces, with a strong correlation between these parameters and soil response observed through comprehensive dynamic analysis. Moreover, the comparison between the experimental and numerical results confirms the high accuracy and reliability of the developed model, showing that soil behavior follows consistent patterns with respect to variations in rake angle and depth, regardless of tool geometry or cutting velocity. These findings highlight that the proposed numerical model provides a deeper theoretical understanding of soil-cutting mechanics and enhances the ability to predict and optimize excavation performance under different operating conditions.

MATERIAL AND METHODS

The research approach combined experimental investigation and numerical modeling to study the mechanical response of soil during excavation. The work was structured in four stages: (i) defining the geometry and material properties of the excavation tool, (ii) characterizing the clayey sand soil through laboratory testing, (iii) performing controlled soil bin experiments to measure excavation forces, and (iv) developing a three-dimensional SPH model in Abaqus Explicit to

reproduce and analyze soil-tool interaction. Each stage is described in the following subsections.

Excavation tool geometry and material properties

Excavator bucket teeth in the mining sector are typically manufactured from robust alloy steels to withstand demanding operating conditions [24]. Despite their strength, these teeth are highly exposed to abrasive forces, making them susceptible to damage and wear during service. To improve durability, hard-facing with wear-resistant materials is often applied, extending service life under abrasive environments [25]. Nevertheless, even hard alloys may show insufficient resistance over prolonged use, which has led to growing interest in surface coatings as a practical solution for enhancing wear performance [26].

In the present study, a bucket tooth was modeled in three dimensions using SOLIDWORKS 2022, based on the real geometry of a CAT K130 (220-9133) tooth as shown in (Figure 1). The main geometrical dimensions of the bucket tooth employed in the numerical simulation are listed in Table 1. Table 2 presents the mechanical properties of the EN X200Cr12 steel grade used for the fabrication of the CAT K130 (220-9133) bucket tooth, these parameters were used to define the material behavior of the excavation tool in the simulation.

Soil characterization and model calibration for numerical analysis

Soil constitutive models are developed to capture different soil types and loading conditions. Advanced models such as the Cam-Clay model simulate soil response under complex stress paths [27], while the hardened soil (HS) and hardened soil with small strain (HSS) models improve predictions of stiffness and deformation behavior. Despite these advances, the MC model remains widely used in geotechnical applications, since differences in safety factors and predicted forces compared with advanced models are often limited. The MC model represents soil shear strength through two main parameters, cohesion and internal friction angle, making it both practical and straightforward for engineering use [28]. Its popularity is also linked to the simplicity of determining these parameters through standard in situ or laboratory tests [29]. To improve accuracy,

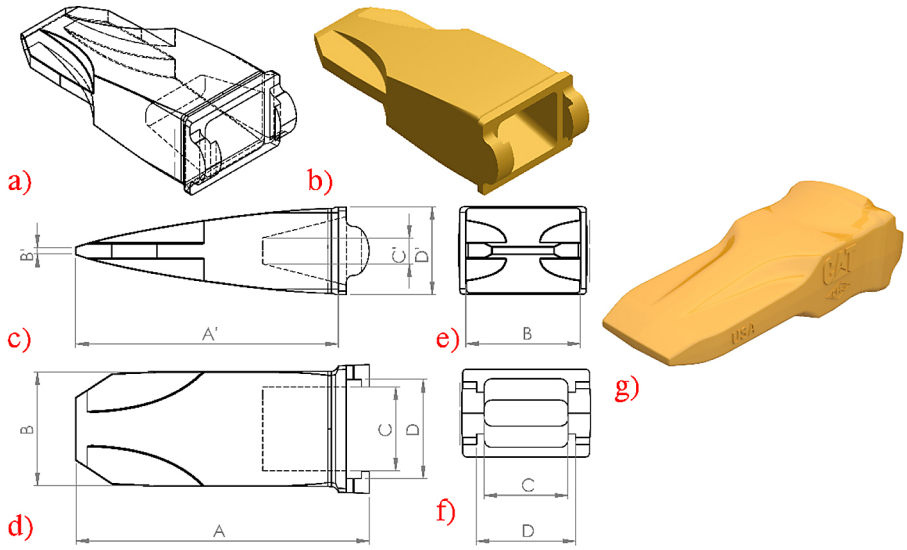

Figure 1. Three-dimensional model of the CAT K130 (220-9133) bucket tooth generated in SOLIDWORKS 2022 for use in excavation tool simulations: (a, b) 3D view, (c) side view, (d) top view, (e) front view, (f) back view, (g) Reel CAT K130 tooth

Table 1. Geometrical dimensions of the CAT K130 (220-9133) bucket tooth used in the excavation tool simulations (mm)

A	B	C	D	A'	B'	C'	D'
386	150	110	130	346	10	34	115

Table 2. Mechanical properties of the CAT K130 (220-9133) bucket tooth material considered in the numerical model

Material	EN: X200Cr12
Elastic modulus (MPa)	207000
Mass density (kg.m^{-3})	7700
Poisson's ratio	0.3
Yield strength (MPa)	976
Hardness (HB)	250

modified forms of the MC model have been developed to incorporate nonlinear elasticity [30] as well as hardening and softening effects [31], enabling more realistic predictions of soil behavior under excavation or other loading conditions.

Coulomb proposed a soil pressure theory of soil or rock failure, expressed as:

$$\tau = c - \sigma \ tan\,\varphi \tag{1}$$

where: τ – shear strength acting on the failure plane (MPa), σ – normal stress on the failure plane with tensile stress considered positive (MPa), c – cohesion of the soil or rock (MPa), φ – internal friction angle (°).

Later, Mohr developed this condition into the law of shear failure, known as the Mohr-Coulomb yield criterion (Figure 2), which may be expressed in terms of the principal stresses ($\sigma_1 \leq \sigma_2 \leq \sigma_3$) as:

$$\sigma_1 = \frac{1}{2}(\sigma_1 + \sigma_3) - \frac{1}{2}(\sigma_1 - \sigma_3)\,sin\,\varphi \tag{2}$$

where: σ_1 – major principal stress at failure (MPa), σ_3 – minor principal stress at failure (MPa).

Equation 2 defines the relationship between the shear strength parameters (c, φ) and the stress state at failure. The Mohr-Coulomb model is a first-order elastic-perfectly plastic formulation that is frequently applied to simulate soil behavior [32]. Its main advantage lies in the small number of input parameters required, which makes it practical for a wide range of engineering applications [33]. The model provides a well-defined failure criterion based on shear strength, enabling consistent prediction of soil response under loading [34]. Experimental studies have confirmed that the Mohr-Coulomb yield criterion adequately represents the failure behavior of soils and rocks under diverse conditions [35]. In this research, clayey sand soil was analyzed through three-dimensional dynamic modeling supported by laboratory experiments. X-ray diffraction (XRD) was performed to determine the mineralogical composition of the soil. The direct shear test (Casagrande method) was used to obtain the shear strength parameters cohesion (c), internal friction angle (φ), and dilatancy angle (ψ), which are summarized in Table 3. These results were then incorporated into the numerical model to provide a reliable basis for simulating soil-tool interaction.

Table 3. Mechanical properties of the clayey sand soil determined from Casagrande shear tests

Mechanical properties	Soil
Elastic modulus (MPa)	28
Mass density (kg.m^{-3})	1790
Poisson's ratio	0.32
Cohesion (KPa)	8
Internal friction angle (φ)	30°
Dilatancy angle (ψ)	0°
Water content (%)	15.84

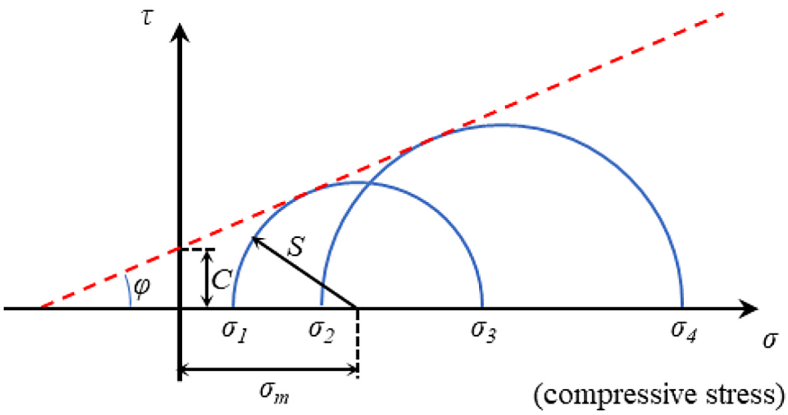

Figure 2. Schematic of the Mohr-Coulomb yield surface in principal stress space [36]

Experimental setup and testing procedure

The experimental tests were carried out at the Soil Bin Testing Facility, which is designed to study the soil-tool interactions under controlled laboratory conditions, as shown in Figure. 3. The bin dimensions were 5000 mm in length, 3000 mm in width, and 1600 mm in depth, allowing realistic simulation of excavation processes while maintaining full control over the influencing parameters.

The excavation tool was a bucket tooth mounted on a rigid, adjustable holder, which permitted precise modification of the rake angle to 30°, 45°, 60°, 75°, and 90°. The tool was attached to a horizontally moving carriage operating at a constant speed of 100 mm/s. Cutting depth was adjustable to 100 mm, 150 mm, 200 mm, 250 mm, and 300 mm, which allowed systematic assessment of depth effects on excavation forces.

The soil used in the test was clayey sand, with mechanical properties summarized in Table 3. Prior to each run, the soil bed was prepared to achieve uniform density and moisture distribution across the bin. This preparation involved controlled compaction and leveling, ensuring consistent and repeatable conditions for all trials.

During testing, the bucket tooth traveled along the full length of the bin so that steady-state excavation was reached before data collection. The forces acting on the tool were measured with calibrated load cells, which independently recorded the horizontal force (draft) and the vertical force (penetration). Data were acquired through a computer-based logging system at a sampling rate of 50 Hz, producing detailed force-time curves. Each combination of rake angle and cutting depth was repeated three times, and the average values were calculated to reduce random error as well as ensure measurement consistency.

Numerical modeling of soil-tool interaction using SPH

Smoothed particle hydrodynamics (SPH) has been increasingly applied to model soil deformation, stress distribution, and failure mechanisms during excavation tool interactions. Compared to computational techniques such as the FEM, which discretizes the soil as a mesh of elements, or the discrete element method (DEM), which represents soil and soil-rock mixtures as particles [37], SPH is a mesh-free particle-based approach that effectively handles large deformations and material separation without mesh distortion [38]. Previous studies have shown that SPH can more accurately simulate the forward movement of soil below the cutting depth due to its ability to capture free surfaces and soil flow [20].

The three-dimensional soil-tool interaction model in this study was developed in Abaqus Explicit using SPH. The model consisted of two components: (i) the Caterpillar bucket tooth K130 (220-9133), modeled as a rigid cutting body, and (ii) the soil domain, represented by SPH particles to reproduce the mechanical response of clayey sand. The reported soil domain dimensions vary considerably across studies depending on tool geometry and modeling objectives, ranging from 300 × 300 × 100 mm [39] to 900 × 900 × 700 mm [40]. These differences highlight the importance of choosing domain sizes proportional to tool scale.

Here, a soil bin with dimensions of 700 × 400 × 500 mm was selected to represent clayey sand. The same geometry and soil properties were applied in both the experimental tests and the SPH model, allowing direct comparison between numerical and laboratory results. The soil was modeled as isotropic, and to maintain stability, SPH particles at the far boundaries were fixed in all

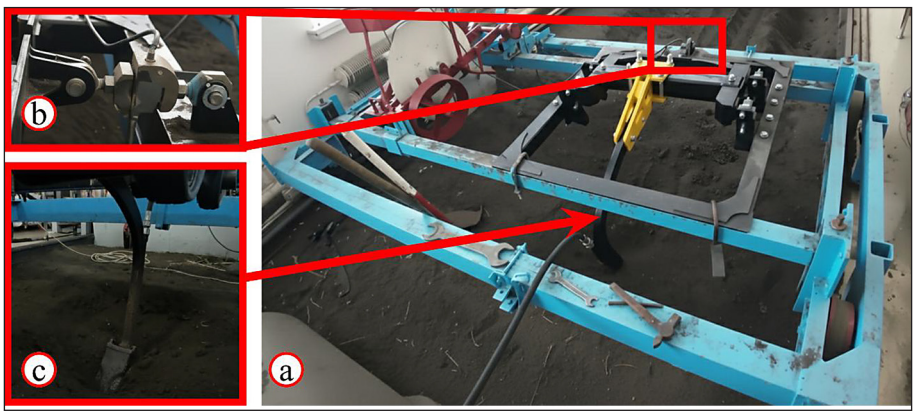

Figure 3. (a) Soil bin testing, (b) load cells "force sensors", (c) cutting tool rigid mount

degrees of freedom to prevent drift. This configuration ensured consistency between experiments and simulations while preserving computational accuracy and physical realism.

The analysis focused on the influence of rake angle and penetration depth on reaction forces and tool displacement. The tool was driven at a constant velocity of 100 mm/s along the Z direction, with the cutting angle (γ) kept fixed [41]. Two sets of simulations were carried out: (i) angle variation tests at a constant depth of 100 mm, with rake angles of 30°, 45°, 60°, 75°, and 90°; and (ii) depth variation tests at 100, 150, 200, 250, and 300 mm, with the rake angle fixed at 45°, identified from the angle variation series as producing the lowest reaction forces.

Meshing strategy and application of boundary conditions

In Abaqus Explicit, the bucket tooth was meshed using quadratic tetrahedral elements (C3D10) due to its complex geometry. The final finite element model of the tooth consisted of 239,695 elements and 345,333 nodes. The soil bin was initially meshed with hexahedral elements (C3D8R), comprising 108,800 elements and 115,989 nodes. At the initial step, this finite element mesh was converted into SPH particles, and a corresponding SPH particle file was generated as well as imported into the Part module. The resulting SPH soil model used for the soil-tool interaction analysis is shown in Figure 4.

The soil was constrained so that the bottom surface was completely fixed to prevent movement or rotation, simulating a rigid support as the base. The left and right planes were constrained in the X and Y directions to prevent lateral movement and represent confined boundaries. In contrast, the top, front, and back surfaces were left free, allowing natural soil deformation (Figure 4).

A constant translational velocity in the Z direction was applied to the reference point of the bucket tooth, while the other degrees of freedom remained fixed [42]. The analysis was conducted in two explicit calculation stages: an initial step to apply boundary conditions, followed by an explicit dynamic step with a duration of 1 second. These conditions were selected to reproduce realistic soil-tool interaction behavior, consistent with earlier studies [43, 44].

The following diagram (Figure 5) presents the workflow of simulation and experimental validation of the excavation process. It outlines the sequential stages, from numerical model setup and parameter definition to laboratory testing and comparison of results. This representation provides methodological clarity and strengthens the reliability of the soil-tool interaction analysis.

RESULTS AND DISCUSSION

This section presents a comparative analysis of the simulation and experimental results to evaluate the predictive accuracy of the SPH-based numerical model. The study focused on two primary factors governing soil-tool interaction: the rake angle and the excavation depth. Each parameter was examined separately to identify its influence on reaction forces and soil displacement, as well as to determine the conditions that yield the most stable and efficient cutting performance. The following subsections detail these effects and compare numerical predictions with experimental measurements to assess the model's consistency and physical relevance.

Effect of rake angle on reaction forces and soil displacement

The results in Figure 6 show the variation of reaction forces with tool displacement at different rake angles for a constant depth of 100 mm, comparing numerical simulations with experimental measurements. The vertical force (Figure. 6a)

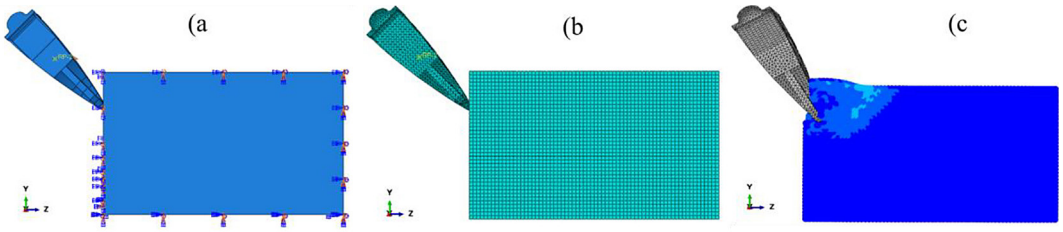

Figure 4. Finite element meshing and boundary conditions applied in the soil-tool interaction model: (a) boundary constraints, (b) soil and tool configuration before excavation, (c) deformation after excavation

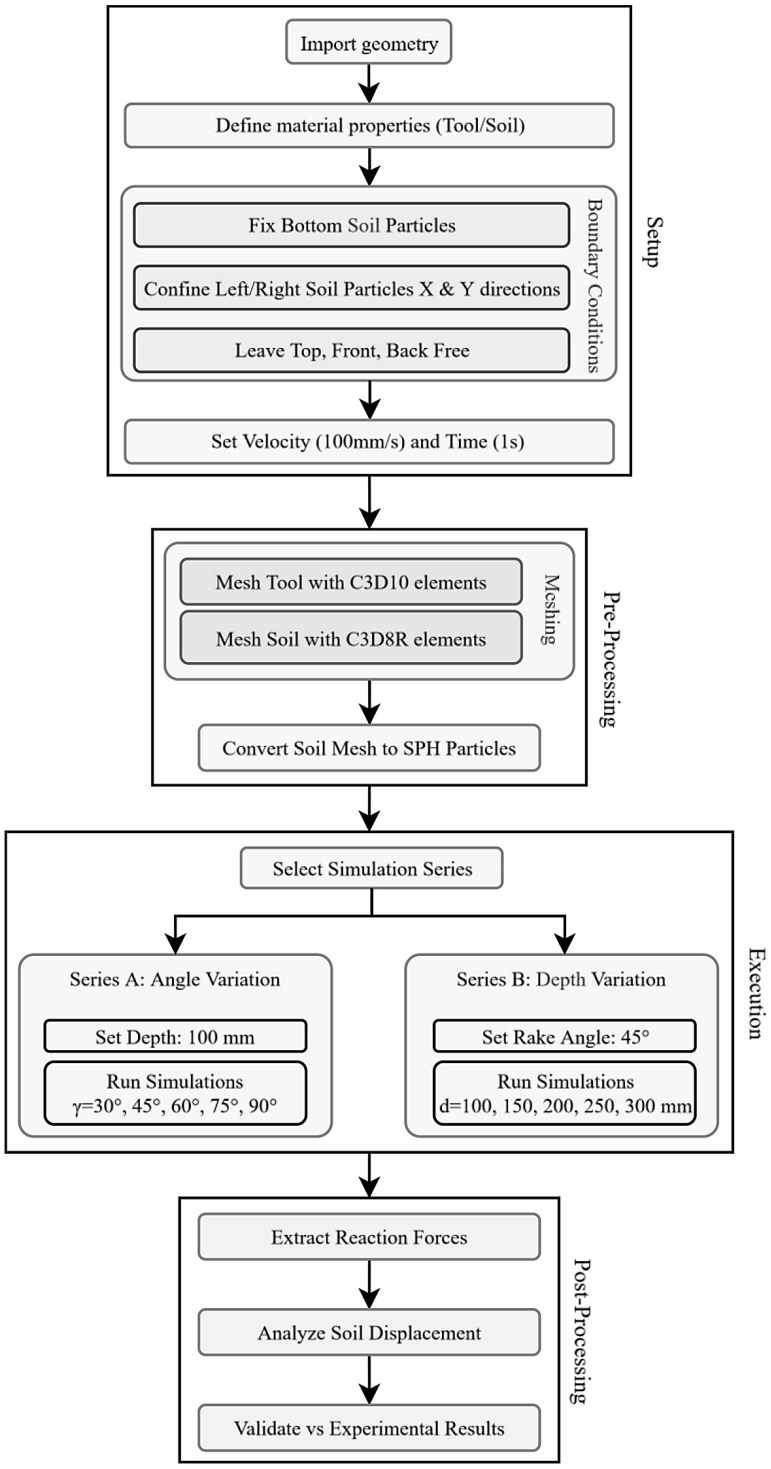

Figure 5. Simulation and experimental validation workflow diagram

decreases continuously, starting close to zero and becoming more negative as displacement increases. At rake angles of 30°, 45°, and 60°, the values converge, while at 75° and 90° the vertical forces reach nearly -500 N, indicating stronger downward resistance from the soil. This trend confirms that soil reaction intensifies with displacement as tool-soil interaction develops. Experimental measurements follow the same pattern as simulations, validating the numerical model and its ability to reproduce soil cutting mechanics.

The horizontal force (Figure 6b) increases steadily with displacement. At 30° and 45°, draft forces remain lower, while at 75° and 90° they rise significantly, exceeding 900 N. This indicates that forward soil resistance grows with

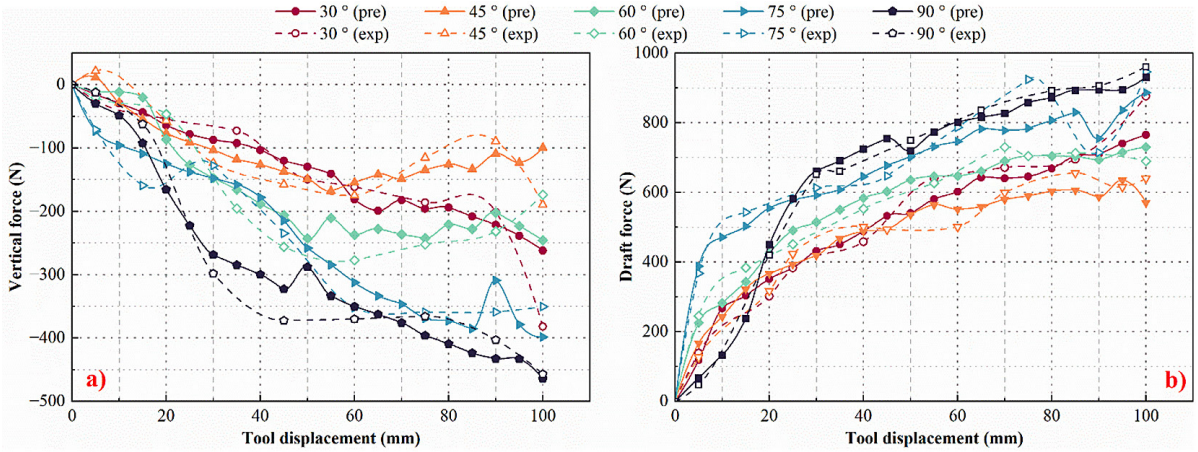

Figure 6. Influence of rake angle on soil reaction force variation at a cutting depth of 100 mm, comparing simulation and experimental results: (a) vertical force (RF2), (b) horizontal force (RF3)

tool advancement and is amplified at higher rake angles due to greater compaction and soil accumulation. Experimental results are in good agreement with simulations, further confirming model reliability. These findings are consistent with soil cutting mechanics, where penetration is easier at the start but resistance grows as cutting progresses, in line with the reported results [45]. The variation of maximum reaction forces with rake angle is summarized in Figure 7. The vertical force (RF2) remains negative at all rake angles, with the smallest magnitude observed at 45 and decreases to nearly -500 N at 90°. This shows that intermediate rake angles reduce downward soil resistance, while higher angles intensify it due to increased soil pressure on the tool. Conversely, the horizontal force (RF3) decreases slightly up to 45°, then increases steadily, reaching its maximum at 90°. This indicates that draft resistance rises at steeper angles. These findings demonstrate that intermediate rake angles provide more favorable cutting conditions by minimizing both vertical and horizontal resistance. The strong agreement between experimental measurements and simulation results confirms the reliability of the numerical model and is consistent with the previous studies [46, 47] which emphasized the strong influence of rake angle on soil-tool interaction.

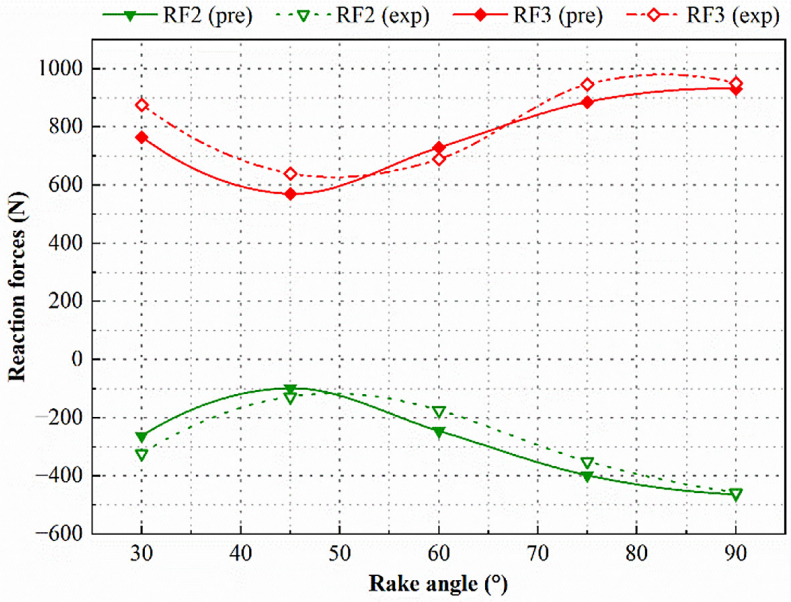

Figure 7. Maximum vertical (RF2) and horizontal (RF3) reaction forces as functions of rake angle, comparing numerical predictions with experimental measurements

Effect of excavation depth on soil reaction and tool performance

In this section, the rake angle is fixed at 45°, identified previously as the optimum value due to higher displacement (greater than 100 mm) and lower reaction forces compared with other angles. Figure 8 presents the vertical (RF2) and horizontal (RF3) reaction forces obtained from both experimental and simulation results, showing close agreement. In Figure 8a, the vertical force is negative at shallow depths of 100 mm and 150 mm, while at greater depths (200–300 mm) it becomes positive and increases in magnitude, indicating that uplift resistance grows significantly with penetration depth. In Figure 8b, the horizontal force rises progressively with displacement for all depths, with maximum values ranging from about 500 N at 100 mm to nearly 1500 N at 300 mm. Although simulations slightly overestimate experimental values at deeper cuts, both sets of results follow the same trend, confirming that excavation depth strongly influences soil resistance. These findings also demonstrate the ability of the numerical model to reproduce the soil-tool interaction behavior. The effect of depth on maximum reaction forces is shown in Figure 9, comparing simulation and experimental data. Both approaches reveal the same trend, with deeper penetration producing progressively higher vertical and horizontal forces. This observation is consistent with [48] and [49], which reported stronger resistances at greater depths. The agreement between the two approaches validates the accuracy of the SPH-based numerical model. Quantitatively, the horizontal force (RF3) rises steadily with depth, reaching approximately 1102 N at 200 mm, 1150.4 N at 250 mm, and 1156.05 N at 300 mm. Similarly, the vertical force (RF2) increases gradually, attaining a maximum of 481.99 N at 300 mm.

Quantitative assessment of simulation-experiment agreement

The comparative evaluation presented in Table 4 demonstrates that the developed dynamic model provides a robust predictive framework for soil-tool interaction. The agreement for horizontal reaction forces (RF3) is particularly strong, with errors below 9% across depths and below 8% across rake angles, supported by high correlation values ($R^2 \approx 0.85$ and 0.73). This indicates that the model consistently reproduces both the magnitude and the evolution of draft forces, making it a reliable tool for assessing excavation performance under varying operating conditions. The results also show that horizontal forces are more accurately captured than vertical forces, which aligns with the findings from previous studies that identified draft force prediction as more stable and reproducible than vertical force estimation [50–51].

For vertical forces (RF2), although the mean absolute error across depths is higher (~62%), the correlation remains strong ($R^2 \approx 0.89$). This suggests that the model captures the overall trend of vertical force development, even if deviations occur at certain depths. Such variability is consistent with the challenges previously highlighted in soil-tool interaction research, where vertical forces are known to be more difficult to predict due to soil heave, detachment effects, and the sensitivity

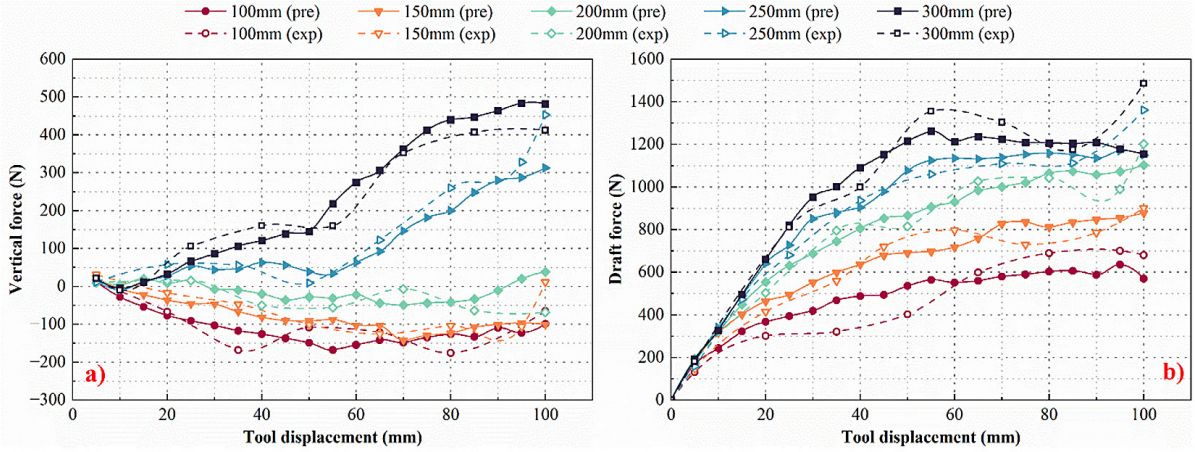

Figure 8. Variation of vertical (RF2) and horizontal (RF3) reaction forces with tool displacement at different penetration depths (100–300 mm) under a fixed rake angle of 45°, showing comparison between simulation and experimental results

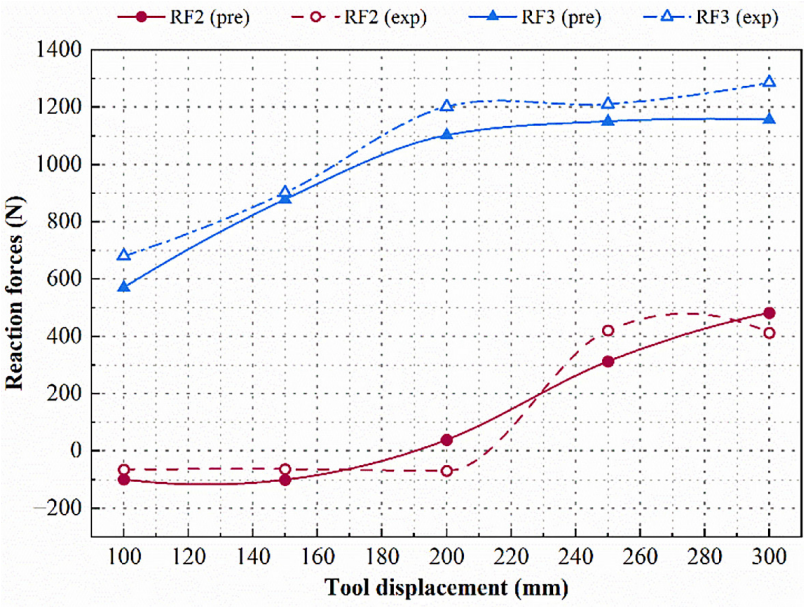

Figure 9. Maximum vertical (RF2) and horizontal (RF3) reaction forces as functions of penetration depth (100–300 mm), comparing numerical predictions with experimental measurements

Table 4. Quantitative comparison between simulated and experimental reaction forces obtained under different operating conditions. RF2 corresponds to the vertical reaction force and RF3 to the horizontal reaction force. The mean absolute percentage error (MAPE) expresses the average deviation between predicted and measured values, while the coefficient of determination (R^2) measures the strength of the correlation. Depth variation refers to tests performed at different penetration depths, and rake angle variation refers to tests at different tool rake angles

Operating condition	Force component	MAPE (%)	R^2	Comment
Depth variation (100 to 300 mm)	RF2: Vertical reaction force	61.76	0.890	Strong correlation but higher deviation due to soil heave and detachment effects
	RF3: Horizontal reaction force	8.76	0.850	Low error and stable correlation, accurate prediction of draft forces
Rake angle variation (30 to 90°)	RF2: Vertical reaction force	19.25	0.836	Consistent trend captured with moderate deviation
	RF3: Horizontal reaction force	7.95	0.733	Acceptable agreement, force evolution well reproduced

Note: the coefficient of determination (R^2) measures the agreement between predicted and experimental results. It ranges from 0 to 1, with values near 1 indicating strong correlation and high model accuracy. In soil-tool interaction studies, $R^2>0.8$ denotes excellent agreement, while $0.6\leq R^2\leq 0.80$ indicates good consistency suitable for engineering use.

of soil response to geometric parameters [52, 53]. Importantly, the present model reduces these limitations by maintaining high correlation values and reproducing the expected force evolution across both depth and rake angle variations.

Taken together, the results confirm that the proposed model is both accurate and generalizable, with high reliability for horizontal forces and consistent performance for vertical force trends. Compared to earlier approaches that struggled with large errors in vertical force prediction or significant instabilities in SPH-based simulations [49, 53], the current model demonstrates a clear advancement by achieving closer agreement with experimental results and offering a validated framework for excavation process simulation. This establishes the model as a significant contribution to soil-tool interaction studies, bridging the gaps observed in past numerical and semi-empirical approaches while enhancing predictive capacity for engineering applications.

CONCLUSIONS

This study investigated the interaction between an excavation tool and clayey sand soil through three-dimensional dynamic modeling

using the smoothed particle hydrodynamics (SPH) method, supported by experimental validation. The effects of rake angle and penetration depth on excavation performance were analyzed systematically. Results showed that depths of 100–150 mm combined with rake angles between 30° and 60° minimized reaction forces while enabling efficient soil displacement. The depth/rake angle couple of 100 mm/45° is identified as the most favorable for balancing excavation efficiency and structural performance of the tool. The numerical predictions showed close agreement with the experimental data, particularly for horizontal reaction forces (RF3), where errors remained below 9% across depths and 8% across rake angles, with strong correlation values. Although vertical reaction forces (RF2) displayed higher variability due to soil heave and uplift mechanisms, the model consistently captured their trends with correlation values above 0.84. This demonstrates that the approach not only reproduces the evolution of draft forces with high accuracy, but also advances the reliability of vertical force predictions, an area where previous models have often struggled.

Compared with the earlier works reporting large discrepancies in vertical force estimation, the present study establishes a validated framework capable of simultaneously predicting horizontal and vertical forces with improved consistency. By identifying the operational ranges that reduce soil resistance while maintaining effective soil failure, the model provides valuable guidelines for optimizing tool geometry and operating conditions. These findings contribute to reducing energy consumption and improving excavation performance under clayey sand conditions, while also laying the groundwork for future extensions to different soils and more complex dynamic loading environments.

REFERENCES

1. Das, B. M. Principles of Geotechnical Engineering. 7th ed., Cengage Learning, 2006.
2. Olsen T., Kasper T., and De Wit J., Immersed tunnels in soft soil conditions: Experience from the last 20 years, Tunnelling and Underground Space Technology, March 2022;121:104315. https://doi.org/10.1016/j.tust.2021.104315
3. Bilgin N., Copur H., and Balci C., Mechanical excavation in mining and civil industries (CRC Press, 2013).
4. Liu, G. R., Liu, M. B. Smoothed particle hydrodynamics: a Meshfree particle method. World Scientific, 2010.
5. Zhang L., Cai Z., Wang L., Zhang R., and Liu H., Coupled Eulerian-Lagrangian finite element method for simulating soil-tool interaction, Biosystems Engineering, November 2018;175:96–105. https://doi.org/10.1016/j.biosystemseng.2018.09.003
6. Chen, W. F., Mizuno, E. Nonlinear analysis in soil mechanics: theory and implementation. Elsevier, 1990.
7. Duncan, J. M., Wright, S. G., Brandon, T. L. (2014). Soil strength and slope stability. John Wiley & Sons).
8. Lambe, T. W., Whitman, R. V. Soil Mechanics. John Wiley & Sons, 2013.
9. Kay B. D., and Angers D. A., Soil structure (CRC Press, 2001).
10. Ma H., Hao X., Yang Y., Li H., and Yi L., Study on parameters of Modified Mohr-Coulomb model for water-rich soft soil in Tianjin, China, SN Applied Sciences, June 2023;5(7):187. https://doi.org/10.1007/s42452-023-05411-x
11. Hayslip M. W., Excavation and trenching, (Handbook of Loss Prevention Engineering, 2013;1:159–199. https://doi.org/10.1002/9783527650644.ch8
12. Galloway D. F., Some experiments on the influence of various factors on drill performance, Transactions of the American Society of Mechanical Engineers, February 2022;79(2):191–224. https://doi.org/10.1115/1.4012963
13. Zienkiewicz, O. C., Taylor, R. L. The Finite Element Method: Its Basis and Fundamentals. 6th ed., Butterworth-Heinemann, 2005.
14. Brinkgreve, R. B. J., Engin, E. Numerical Methods in Geotechnical Engineering. CRC Press, 2013.
15. Nakai, T. Constitutive modeling of geomaterials: principles and applications. CRC press.). 2012.
16. Desai, C. S., Faruque, M. O. Constitutive model for (geological) materials. Journal of Engineering Mechanics, 1984;110(9),1391–1408. https://doi.org/10.1061/(ASCE)0733-9399(1984)110:9(13
17. Griffiths D. V. and Lane P. A., Slope stability analysis by finite elements, Géotechnique, June 1999;49(3):387–403. https://doi.org/10.1680/geot.1999.49.3.387
18. Azizi F., Applied analyses in geotechnics (CRC Press, 1999). https://doi.org/10.1201/9781315274393
19. Chen, W. F. Limit analysis and soil plasticity. Elsevier, 2013.
20. Monaghan, J. J. Smoothed particle hydrodynamics. Annual Review of Astronomy and Astrophysics 1992;30:543–574. https://doi.org/10.1088/0034-4885/68/8/R01
21. Islam, M. R., Rahman, M. A., Hayano, K. Application of smoothed particle hydrodynamics (SPH) for simulating various geotechnical problems. SN Applied Sciences, 2020;2(4):687. https://doi.

org/10.1007/s42452-020-2379-y

22. Maciejewski J., Jarzębowski A., and Trampczyński W., Study on the efficiency of the digging process using the model of excavator bucket, Journal of Terramechanics, October 2003;40(4):221–233. https://doi.org/10.1016/j.jterra.2003.12.003
23. Brinkgreve R. B., and Post M., Geotechnical ultimate limit state design using finite elements, IOS Press, 2015;464–469. https://doi.org/10.3233/978-1-61499-580-7-464
24. Ismail R., Muhammad Z., Jamari J., and Bayuseno A. P., Designing and wear testing of excavator bucket teeth for the need of Indonesian mining, ARPN Journal of Engineering and Applied Sciences, January 2020;15(1):21–26.
25. Dong Z., Jiang F., Tan Y., Wang F., Ma R., and Liu J., Review of the modeling methods of bucket tooth wear for construction machinery, Lubricants, June 2023;11(6):253. https://doi.org/10.3390/lubricants11060253
26. Keleş A., and Yildirim M., Improvement of mechanical properties by means of titanium alloying to steel teeth used in the excavator, Engineering Science and Technology, an International Journal, October 2020;23(5):1208–1213. https://doi.org/10.1016/j.jestch.2019.12.003
27. Cassiani G., Brovelli A., and Hueckel T., A strain-rate-dependent modified Cam-Clay model for the simulation of soil/rock compaction, Geomechanics for Energy and the Environment, September 2017;11:42–51. https://doi.org/10.1016/j.gete.2017.07.001
28. Liang D. F., and He X. Z., A comparison of conventional and shear-rate dependent Mohr-Coulomb models for simulating landslides, Journal of Mountain Science, November 2014;11:1478–1490. https://doi.org/10.1007/s11629-014-3041-1
29. Tian D., and Zheng H., The generalized Mohr-Coulomb failure criterion, Applied Sciences, April 2023;13(9):5405. https://doi.org/10.3390/app13095405
30. Rajmeny P. K., Jain P. K., and Abouzar V., 3D-numerical simulation of a mine using cohesion-softening, friction-softening and hardening behavior (Atlantis Press, November 2016;11–20. https://doi.org/10.2991/rare-16.2016.2
31. Meng X., Geng D., and Liu S., The modified Mohr-Coulomb model considering softening effect and intermediate principal stress, Mechanics of Advanced Materials and Structures, August 2024;32(11):1–15. https://doi.org/10.1080/15376494.2024.2380384
32. Ti K. S., Huat B. B., Noorzaei J., Jaafar M. S., and Sew G. S., A review of basic soil constitutive models for geotechnical application, Electronic Journal of Geotechnical Engineering, 2009;14:1–18,
33. Robert D. J., A modified Mohr-Coulomb model to simulate the behavior of pipelines in unsaturated soils, Computers and Geotechnics, November 2017;91:146–160. https://doi.org/10.1016/j.compgeo.2017.07.004
34. Li X., Finite element analysis of slope stability using a nonlinear failure criterion, Computers and Geotechnics, May 2007;34(3):127–136, https://doi.org/10.1016/j.compgeo.2006.11.005
35. Xiang X., and Zi-Hang D., Numerical implementation of a modified Mohr-Coulomb model and its application in slope stability analysis, Journal of Modern Transportation, March 2017;25:40–51. https://doi.org/10.1007/s40534-017-0123-0
36. Zaid, M., Sadique, M.R. Samanta, M. Effect of unconfined compressive strength of rock on dynamic response of shallow unlined tunnel. SN Appl. Sci. 2020;2:2131 https://doi.org/10.1007/s42452-020-03876-8
37. Ucgul M., Saunders C., and Fielke J. M., Comparison of the discrete element and finite element methods to model the interaction of soil and tool cutting edge, Biosystems Engineering, May 2018;169:199–208. https://doi.org/10.1016/j.biosystemseng.2018.03.003
38. Bui, Ha H., et al. Lagrangian meshfree particles method (SPH) for large deformation and failure flows of geomaterial using elastic-plastic soil constitutive model. International journal for numerical and analytical methods in geomechanics 2008;32(12):1537–1570. https://doi.org/10.1002/nag.688
39. Tagar A. A., Changying J., Adamowski J., Malard J., Qi C. S., Qishuo D., and Abbasi, N. A. Finite element simulation of soil failure patterns under soil bin and field-testing conditions, Soil and Tillage Research, January 2015;145:157–170, https://doi.org/10.1016/j.still.2014.09.006
40. Ibrahmi A., Bentaher H., and Maalej A., Soil-BLADE orientation effect on tillage forces determined by 3D finite element models, Spanish Journal of Agricultural Research, 2014;12(4):941–951, https://doi.org/10.5424/sjar/2014124-5766
41. Abo-Elnor M., Hamilton R., andBoyle J. T., 3D dynamic analysis of soil-tool interaction using the finite element method, Journal of Terramechanics, January 2003;40(1):51–62, https://doi.org/10.1016/j.jterra.2003.09.002
42. Abo-Elnor M., Hamilton R., and Boyle J. T., Simulation of soil-BLADE interaction for sandy soil using advanced 3D finite element analysis, Soil and Tillage Research, January 2004;75(1):61–73, https://doi.org/10.1016/S0167-1987(03)00156-9
43. A.Armin, R. Fotouhi, and W. Szyszkowski, On the FE modeling of soil-BLADE interaction in tillage operations, Finite Elements in Analysis and Design, December 2014;92:1–11, https://doi.org/10.1016/j.finel.2014.07.004

44. Godwin R. J., and O'Dogherty M. J., Integrated soil tillage force prediction models, Journal of Terramechanics, January 2007;44(1):3–14, https://doi.org/10.1016/j.jterra.2006.01.001
45. Tong J., and Moayad B. Z., Effects of rake angle of chisel plough on soil cutting factors and power requirements: A computer simulation, Soil and Tillage Research, July 2006;88(1–2):55–64, https://doi.org/10.1016/j.still.2005.04.007
46. Manuwa S. I., Ademosun O. C., Agbetoye L. S., and Adesina A., The influence of implements and operational parameters on draught and soil disturbance of model tillage tools, in 2010 ASABE Annual International Meeting, Pittsburgh, Pennsylvania, June 20–23, 2010, American Society of Agricultural and Biological Engineers, 2010. https://doi.org/10.13031/2013.29670
47. Mouazen A.M., and Ramon H., A numerical-statistical hybrid modeling scheme for evaluation of draft requirements of a subsoiler cutting a sandy loam soil, as affected by moisture content, bulk density and depth, Soil and Tillage Research, January 2002;63(3–4):155–165, https://doi.org/10.1016/S0167-1987(01)00243-4
48. Singh J., Chatha S. S., and Sidhu B. S., Influence of tillage depth and plough speed on performance of primary tillage tools, Asian Journal of Engineering and Applied Technology, November 2018;7(S2):138–142, https://doi.org/10.51983/ajeat-2018.7.2.900
49. Perdok U. D. and Kouwenhoven J. K., Soil tillage forces and the design of tillage tools, Soil and Tillage Research, 1994;30(4):293–304, https://doi.org/10.1016/0167-1987(94)90008-6
50. Cheng H., Chen J., Chen R., Huang J., and Li J. Three-dimensional analysis of tunnel face stability in spatially variable soils. Computers and Geotechnics 2019;111:76–88, https://doi.org/10.1016/j.compgeo.2019.03.005
51. Fielke J. M., Interactions of the cutting edge of tillage implements with soil, Journal of Agricultural Engineering Research, 1994;59(2):61–73, https://doi.org/10.1006/jaer.1996.0008
52. Hettiaratchi D. R. P., and Reece A. R. The calculation of passive soil resistance. Geotechnique 1974;24(3):289–310. https://doi.org/10.1680/geot.1974.24.3.289
53. Shmulevich I., State of the art modeling of soil-tillage interaction using discrete and finite element methods, Soil and Tillage Research, 2010;111(1):41–53, https://doi.org/10.1016/j.still.2010.08.003